1 **A simplified system to quantify storage of carbon dioxide, water vapor and heat within a**

2 **maize canopy**

3 Taqi Raza[1*], Bruce B Hicks[1,2], Joel N. Oetting[1] and Neal S Eash[1]

5 [1]Department of Biosystems Engineering and Soil Science, The University of Tennessee, Knoxville

6 USA

7 [2]MetCorps, Norris, USA

9 *Corresponding author: Taqi Raza; taqiraza85@gmail.com, traza@vols.utk.edu

10 Department of Biosystems Engineering and Soil Science, The University of Tennessee, Knoxville

11 USA

13 **Highlights**

14   1. A new multiport system simplifies measuring CO_2 and water vapor gradients in a plant

15   canopy.

16   2. The system eliminates the effects of sensor calibration differences.

17   3. Field tests illustrate the ruggedness of the design, suitable for remote and demanding

18   circumstances.

19   4. Addition of temperature sensors permits application to surface heat storage and energy

20   balance.

22 **Abstract**

23 The canopy storage of CO_2, latent heat and sensible heat within agricultural crops has not yet

24 been fully examined. Reported canopy storage terms are consistently smaller than found for a

25 forest ecosystem, such that they are often neglected. A multiport profile system has been

26 developed to examine these storage terms. The system sequentially samples air from four

27 heights to a single non-dispersive Infrared Gas Analyzer (IRGA). Following extensive laboratory

28 testing, the system has been field proven in an east Tennessee study of a maize crop in 2023.

29 The new system enables quantifications of CO_2 and latent heat atmospheric storage terms and,

30 with supporting temperature measurements, allows improved examination of the surface heat

31 energy budget and the net air-surface exchange of CO_2.

32

33 **Keywords:** Multi-port system, vertical canopy profile, storage terms (CO_2 and heat), energy

34 balance, maize, carbon sequestration

35

36   **1 Introduction**

37 In the last few decades, significant work has attempted to improve our understanding of

38 gaseous exchanges between soils, plants, and the atmosphere. These improvements have been

39 incorporated in land-surface models and numerically-based weather predictions as well as in

40 assessment of atmospheric fluxes of carbon dioxide (Lamas Galdo et al., 2021), water vapor

41 (Wang et al., 2023), and heat over vegetated landscapes (e.g., Hoeltgebaum and Nelson, 2023).

42   Observations of the surface heat budget over forests have shown that the balance

43 expressed by the familiar relationship:

44              $R_n - G = H + LE$ (1)

45 is not always attained. Here, R_n is net radiation, G is soil heat flux, H is sensible heat flux and LE

46 is latent heat flux (q.v. Wilson et al., 2002). Measurements of the turbulent fluxes H and LE are

47 usually by the eddy covariance (EC) methodology (Nicolini et al., 2018), which is also used to

48 measure the flux of carbon dioxide — F_{CO2}. In practice, R_n is measured using well-accepted

49 sensors and ground heat flux plates are installed in the soil to determine G. Routine EC

50 measurements are now made at more than 1000 locations globally (c.v. Fluxnet; Pastorello et

51 al., 2020).

52   An important factor emerging from many experimental studies using eddy covariance is

53 that storage terms contribute substantially to energy closure of vegetated areas and to the

54 quantification of evapotranspiration (McCaughy and Saxton, 1988; Hoeltgebaum and Nelson,

55 2023). In concept, errors in the surface heat balance can be attributed to many additional

56 factors, including omission of the heat used in photosynthesis and the storage of heat in plant

57   biomass, in the air below the height of micrometeorological flux measurement and in the soil

58   layer above the depth of G measurement. If the site in question is not flat, horizontal and

59   homogeneous for a considerable distance upwind, then gravity flows, and advection must be

60   expected to play a role. Investigation of these various contributing factors requires

61   measurement of the relevant variables as they change with space and with time; especially

62   challenging due to temporal (particularly diurnal) changes in air temperature and humidity

63   (Varmaghani et al., 2016) as well as in concentrations of carbon dioxide (herein represented by

64    $[CO_2]$).

65   There are several other possible reasons for energy closure errors in EC

66   experimentation, such as loss of low- or high-frequency flux components, non-optimal

67   coordinate rotation, and the use of inappropriate averaging times (Massman and Lee, 2002;

68   Meyers and Hollinger, 2004; Oetting et al., 2024). Finnigan (2006) reported that the

69   atmospheric heat storage term is underestimated when the average sampling time is large.

70   Neglecting canopy storage terms in studies of Net Ecosystem Exchange (NEE) can also cause

71   substantial errors (Raza et al., 2023). Fewer than 30% of known experimental locations apply a

72   profile measurement system to calculate the temporal variations in storage terms (Papale,

73   2006). Many studies report that energy balance closure is an unsolved problem for a variety of

74   vegetation types: the sum of sensible and latent heat flux is found to be 10-30% lower than the

75   available energy (Wilson et al.,2002; Twine et al.,2000; Leuning et al. 2012; Russell et al. 2015;

76   Raza et al., 2023).

77   In the case of agricultural cropping systems, atmospheric storage terms are usually

78   considered small and are often ignored (Nicolini et al., 2018; Raza et al., 2024). Assessments of

79   storage terms within agricultural ecosystems are few and differ from those well documented by

80   researchers in the case of forest ecosystems studies (Mayocchi and Bristow, 1995; Wilson et al.,

81   2002; Hicks et al., 2020). Most results of heat storage in forest environments focus on the

82   atmospheric component of the total heat storage.

83   The present paper focusses on a resolution to needs for detailed measurement of

84   profiles of water vapor and carbon dioxide concentrations in the atmospheric surface

85   roughness layer, as arose in the decade-long sequence of field studies conducted by the

86   University of Tennessee in Lesotho, Zimbabwe, Ohio and Tennessee (see Eash et al, O'Dell et al;

87   Hicks et al.). The surface roughness layer is that layer of air in contact with the surface below

88   the height at which familiar micrometeorological flux/gradient relationships apply. These

89   studies have concentrated on aspects of the surface energy balance and crop carbon dioxide

90   exchange in areas different from conventional agricultural-meteorology experiments, namely in

91   areas of complex terrain and small plots as confront farming communities in Africa and much of

92   eastern North America. These experiments have increasingly indicated the importance of

93   detailed temperature and concentration measurements in the surface roughness layer.

94   A central requirement has been the need to describe water vapor and CO_2

95   concentrations in more detail than conventional micrometeorology normally provides. To this

96   end, the present paper describes an experimental procedure that builds upon air-sampling

97   systems of the past but is streamlined to provide the requisite measurements with the desired

98   time and space detail, in areas often distant from immediate technical support. Some

99   illustrations of its field utility are provided, using observations from a study of a maize canopy in

100   eastern Tennessee in 2023.

101   **2. Apparatus design and operation**

102   The development described here is an outgrowth of experience with eight preceding field

103   studies, conducted at locations in Lesotho, Zimbabwe, Tennessee, and Ohio (Eash et al., 2013;

104   O'Dell et al., 2014, 2015; Hicks et al., 2021, 2022). These demonstrated the need for a reliable

105   yet technically simple system to measure gas concentrations within and above a growing crop.

106   To satisfy the basic requirements for time continuity and reliability of the data record, a new

107   multi-port sampling system was developed.

108   To avoid consequences of individual sensor offsets when gradients are computed, the

109   new system is designed to use a single detection system, in this case an infrared CO_2/H_2O gas

110   analyzer (IRGA; LI-COR-850, Lincoln, NE). Figure 1 presents a schematic description of the

111   apparatus. The system is designed to maintain continuous airflow through all intake tubes, to

112   cycle through all heights of measurement in one minute (7.5 seconds for each height) and to

113   minimize the switching time between samplings. The system uses two small pumps [Model TD-

114   3LSA, Brailsford & CO., Inc. Antrium. NH, USA], one pump (the purge pump) draws in air at a

115   constant rate through all intake tubes to minimize hygroscopic interactions along the tube

116   walls. Another pump (the sampling pump) pushes the drawn air to the IRGA. The sampling

117   pump is mounted close to the IRGA so that air smoothly enters the IRGA at ambient pressure.

118   When sampling the airflow through a specific tube the flow rate is maintained at 1000 ml min^{-1}.

119   The flow rates through the other three tubes are then maintained at 700 ml min^{-1} by flow

120   meters [LZQ-7 flowmeter, 101.3 KPa, Hilitland, China]. The switching between sampling tubes is

121   controlled by four three-way brass and stainless-steel solenoid valves [231Y-6, Ronkonkoma,

122   NY, USA].
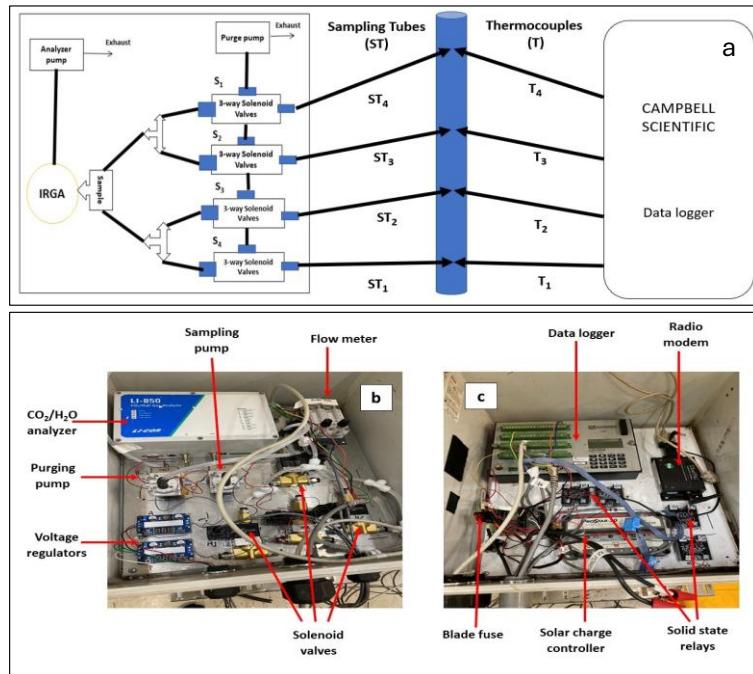
123

124   Fig. 1. Details of the multi-port sampling system: (a) schematic diagram of the manifold for
125   profile sampling of CO_2 and H_2O, (b) a photograph of the analyzer, pump, and manifold
126   system, (c) the data logger for data collection.

127   Each sampling tube is same length (10.5 m), to ensure samples from each sampling

128   height have the same transit time. The purge pump manifold and all sampling tubes are

129   constructed of the same kind of urethane [BEV-A-LINE, Polyethylene material, Cole Parmer,

130   City, State]. Before entering the analyzer, the air is passed through a 1-µm pore filter [LI-6262,

131   LI-COR, Lincoln NE, USA] to avoid the accumulation of debris, dirt, particles, etc., that can cause

132   contamination in the analyzer optical cells. The air outlet of the purge pump and IRGA are open

133   directly to the atmosphere. Digitizing is at 5 Hz frequency. The data system is arranged to

134   record averages and standard deviations at a pre-arranged periodicity, depending on the

135   research goal but typically 5, 10 or 15 minutes.

136   The performance of the system for measurement of CO_2 and H_2O profiles was examined

137   extensively before its field deployment. The apparatus was first flushed with nitrogen (N_2) gas

138   to create a zero-carbon dioxide environment. Subsequently, a known concentration of CO_2 (430

139   ppm) at ambient pressure was fed through the intake tubes sequentially and system outputs

140   were measured. This process allowed determination of the time taken to reach stable

141   measurement readings.

142   To derive a continuous record of concentrations at each height of interest (in the

143   preliminary configuration, four of them) switching between heights was set at every 7.5

144   seconds allowing each of the heights to be sampled twice in every minute. The laboratory tests

145   showed that after the IRGA received a step change in CO_2 concentration it took approximately

146   1.8 seconds to achieve a steady output. During the laboratory evaluation period, the recorded

147   error was less than 0.5% in [CO_2] between sampling heights. An accuracy error of less than 1%

148   is well within the acceptable range for the IRGA now used according to the specifications

149   provided by the manufacturer and much less than higher errors common in measurements of

150   this kind (Montagnani et al. 2018)

151   **3. Field evaluation**

152   An ongoing field study of a maize crop in East Tennessee provided an opportunity to test the

153   new sampling system in experimentally demanding circumstances. The experiment was at a 23

154   ha plot of agricultural farmland, near Philadelphia, in Loudon County Tennessee (35.673° N,

155   84.465° W). The site is typical of agricultural land used for mainly maize and soybean

156 production, in slightly rolling terrain that presents a challenge to EC measurements, with local

157 slope varying from 1% to 5% depending on location. For the present purpose, it is not necessary

158 to provide details of the experiment or of the analysis resulting from it. Such detailed

159 examination of the observations will be presented elsewhere. However, the maize variety was

160 "Dekalb 66-06". The mean annual temperature and precipitation of the site are 13.5 $^{\circ}$C and 140

161 cm respectively. The soil was classified as an Alcoa Loam (fine, thermic Rhodic Paleudult)

162 according to the USDA-NRCS (2018). The experiment extended through the entire growth cycle,

163 from which data for six weeks during the months of May and June 2023 have been extracted

164 for the present illustrative purpose. Maize planting was on 25 April., so that the illustrations to

165 follow relate to a period of rapid growth of the canopy, from soon after emergence (in early

166 May) to tasseling (in June).

167   In the field test considered here, the system was used to measure at heights of 0.11 m,

168 0.5h, 1+h, 2+h, where h is maize canopy height (in meters) above the soil surface. Note that one

169 intake was permanently set at 0.11 m, and the three other heights were adjusted as the maize

170 grew. Sampling intakes were positioned on a 3.5 m steel mast. Thermocouples at the same

171 height as gas sample intakes were used to measure temperature gradients; these were

172 aspirated within a white PVC pipe shield of 1.9 cm diameter (Figure 2a) that also served as a

173 radiation shield.

174   The experimental program hosting this field test utilized a tripod tower to support an

175 eddy covariance system (adjusted as the crop grew to maintain a height about 2 m above the

176 crown) and supporting micrometeorological measurements — an IRGASON [CO_2/H_2O] open

177 path gas analyzer system, [Campbell Scientific, Logan, Utah], a net radiometer [Kipp & Zonen,

178 OTT HydroMet B.V. Delft, Netherlands], infrared radiometers [IRs-S1-111-SS, Apogee

179 Instruments Inc, City, State, USA], and type T thermocouples [Omega, City, State, USA]. The

180 entire observing system was visually inspected every week for signs of leakage, condensation,

181 and contamination. The IRGASON gas analyzer used for eddy covariance was independent of

182 the IRGA used for concentration gradient measurements. The availability of the EC system and

183 its supporting measurements enabled the tests of the new sampling system to extend to

184 investigation of such matters as the height of origin of thermal eddies, as will be reported later.

185
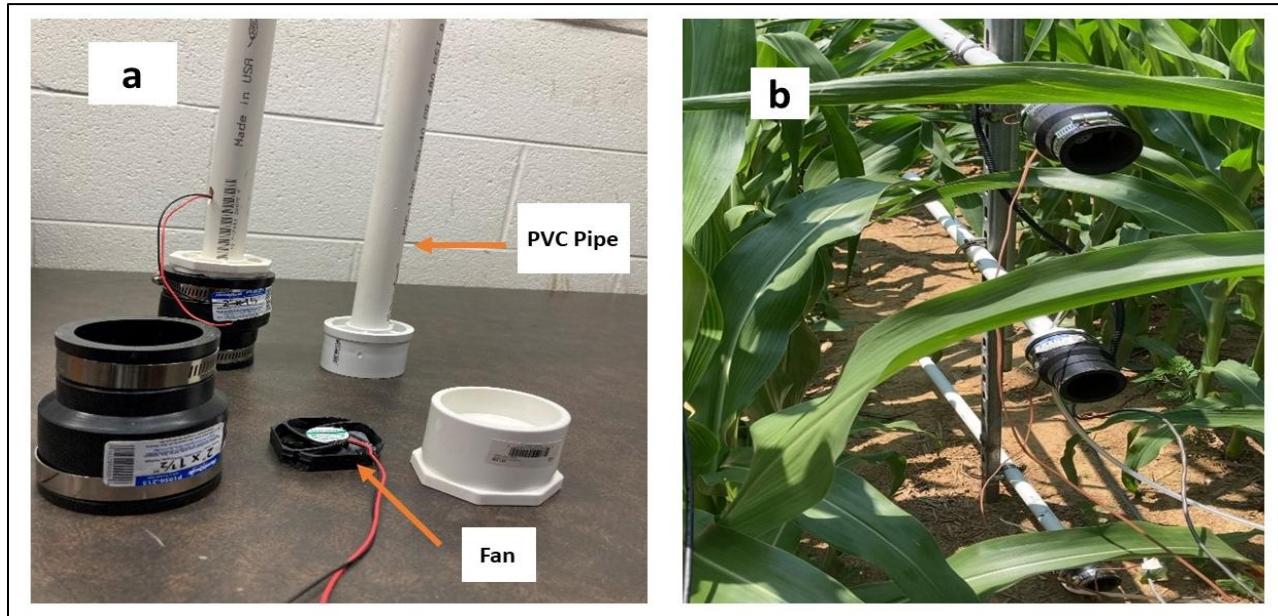
187 Fig. 2. (a) Installation components at each height of the new profile system, showing the
188 aspirated CO_2 intake tubes and thermocouples. (b) Deployment in a maize canopy; the two
189 lowest heights are shown.

190 **3.1. Results — CO_2**

191 Within a nocturnal strongly stratified surface roughness layer, previous experiments have

192 revealed the ubiquity of pooling of CO_2 emitted by soil biota and root respiration. Fig. 3

193 presents average diurnal cycles of CO_2 concentrations measured over the six weeks from 18

194 May to 29 June at four heights, two within the canopy and two above. Error bounds correspond

195 to +/- one standard error of the mean. The variability of CO_2 was found to be higher at

196 nighttime than in daytime. The greatest variability was recorded within the canopy, at height 1

197 (0.11 m) and height 2 (0.4 – 1.4 m).

198   The observations confirm the generally accepted features of nocturnal accumulation of

199 CO_2 effluxes from the soil but with detail sufficient to warrant detailed examination. The close

200 tracking of the records for the different measurement heights provides confidence in the

201 performance of the sampling system and indicates that the same causative mechanisms affect

202 all of the heights similarly. The nighttime results that are plotted support the assumptions

203 made elsewhere that changes in the surface stratified atmosphere are mostly in accord with

204 expectations of CO_2 profile linearity (Galmiche and Hunt, 2002; Verma and Rosenberg, 1976), a

205 result that is supported by close examination of CO_2 averages over shorter nighttime periods.

206
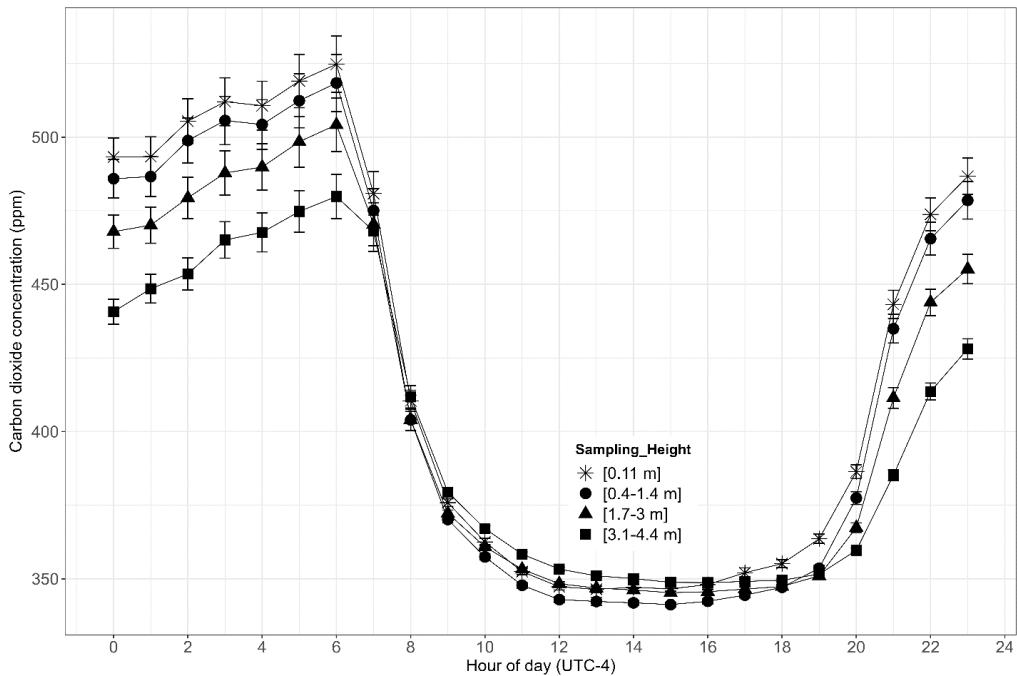
207

208 Fig. 3. Average diurnal cycle of CO_2 obtained using the new system described here, for
209 the six weeks. Symbols correspond to different heights of measurements with error bars
210 corresponding to +/- one standard error.

211 Following 0600 local time, about the average time of sunrise, the average

212 concentrations of CO_2 dropped rapidly as photosynthesis commenced and as convection

213 started to mix surface air with the overlying atmosphere. At all heights this initial decrease was

214 followed by a more rapid loss rate until concentrations dropped to about 350 ppm in the

215 afternoon (1200 to 1800 LT), much lower than ambient concentrations thereby reflecting the

216 efficiency with which the maize crop extracted CO_2 from the air. Near sunset, [CO_2] started to

217   increase and continued to build until reaching maximum values immediately before dawn.

218   Concentrations within the canopy do not differ significantly, although the 0.11 m height values

219   always exceed those further above the soil surface. In general, $[CO_2]$ decreased with increasing

220   height. All of these observations align well with contemporary views of the post-sunrise

221   initiation of photosynthesis and its continuation through the following daylight hours.

222   The nocturnal accumulation of CO_2 observed here is not unusual. In many climatic

223   regions, nighttime soil temperatures remain high enough to sustain microbial and soil

224   respiration activities, resulting in CO_2 accumulation in the stratified air above the ground. After

225   the sun rises, increased light availability increases stomatal activity and photosynthesis rates.

226   **3.2.   Results — H_2O**

227   As in Fig. 3, Fig. 4 shows the average diurnal cycle constructed from 15-minute H_2O

228   concentration observations. At all heights a sharp increase in $[H_2O]$ was recorded in the

229   morning at the same time as the sudden decrease for $[CO_2]$ seen in Fig. 3. Subsequently, $[H_2O]$

230   peaked at about 0900 LT and, within the canopy, maintained this concentration throughout the

231   daylight hours. Above the canopy average concentrations decreased and a different

232   concentration constancy was attained. After the period around sunset had passed, at about

233   2000 LT, $[H_2O]$ started decreasing approximately linearly with time until sunrise approached.

234   The H_2O concentration generally decreased as the measurement height increased for both day

235   and night because a constant source of water vapor was the soil surface, with crop

236   evapotranspiration adding H_2O in the daytime. Dewfall is expected to be important, a

237   contribution that can be uniquely addressed using the new sampling system.

238   Figures 4 and 5 reveal considerably different cycles of CO_2 and H_2O. At night, Fig. 3

239   shows a more striking $[CO_2]$ gradient than does Fig. 4 for $[H_2O]$. The reason is presumed to be

240   that CO_2 continues to be emitted from the soil at night and accumulates within the stratified

241   layer of air, whereas there is no parallel process influencing H_2O concentrations. In daytime,

242   there is little consistent $[CO_2]$ gradient information derivable from Fig. 3, but for $[H_2O]$ in Fig. 4

243   there is a clearly visible $[H_2O]$ gradient structure. This suggests a slow-down of CO_2 exchange in

244   the afternoons while evaporation continued.
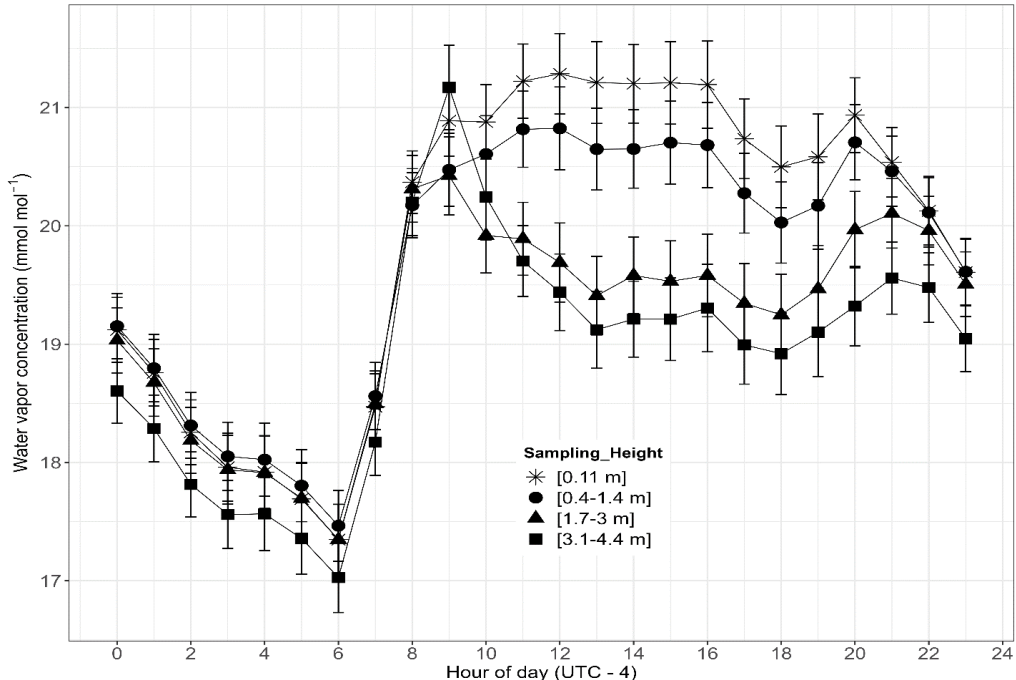
245

246

247   Fig. 4. Average diurnal cycle of the vertical profile of water vapor concentration

248   averaged over six weeks as in Figs. 3. Symbols correspond to different heights of

249   measurements with error bars corresponding to +/- one standard error.

250   The processes of evaporation from the soil surface and evapotranspiration from leaves are

251   linked with solar radiation. Overall, the present results highlight changes in the vertical

252   distribution of water vapor and its temporal variability, indicating near simultaneity of changes

253   on CO_2 and H_2O concentrations following dawn (compare Figs. 3 and 4).

254   **Results — atmospheric storage**

255   The vertical profile data can also be used to explore how various atmospheric storage fluxes

256   influence the CO_2 status and energy budget of the maize crop. In accordance with many

257   studies of the surface energy budget using EC systems, atmospheric storage terms refer to

258   depletion or accumulation of scalar quantities (CO_2, H_2O, etc.) in a hypothetical control volume

259   beneath the height of turbulent flux measurement by EC. A storage flux is defined as the rate

260   of change of dry molar concentrations of the same variables within the same control volume.

261   Both concepts relate most directly to the conditions of "perfect" micrometeorology. In

262   practice, natural complexities of surroundings and exposures interfere to the extent that

263   measurements will be site-specific. Moreover, the covariances are statistical quantities, with

264   well-recognized error margins associated with every quantification of them. During this study,

265   the storage fluxes of scalar quantities (CO_2, water vapor, etc.) were calculated using the ICOS

266   methodology (Montagnani et al., 2018). For the case of CO_2,

267

$$J_c = \overline{\rho_d} \sum_{i=1}^{N} \left(\frac{\Delta c}{\Delta t} \right)_i \Delta z_i. \tag{2}$$

269

270   Here, J_c is the storage term of CO_2 (for example) within the i_{th} layer over which Δc is measured,

271   Δz_i is the thickness of this layer and Δt is the measurement time step; $\overline{\rho}_d$ is dry air density, and

272   N is the number of layers (number of measurements points). To calculate the storage terms as

273   described by Eq. 2, raw data were averaged into 15-minute periods, yielding the results plotted

274   in Fig. 5. CO_2 storage (Fig. 5a) exhibited a larger magnitude and more variation at nighttime

275   compared to daytime, due to the CO_2 pooling and the intermittency of incursions from air aloft.

276   During the night, photosynthesis did not occur, and CO_2 emitted from the soil accumulated in

277   the overlying stratified atmosphere (Ryan and Law, 2005; Davidson and Janssens, 2006). Soon

278   after sunrise, the nighttime stratification began to weaken, and photosynthesis commenced.

279   The trapped CO_2 was consumed by photosynthesis and mixed with air above the canopy as

280   unstable stratification evolved. Minimal CO_2 storage during the daytime can be due to the

281   instability and strong mixing then prevailing, as well as to the photosynthetic removal of CO_2

282   from the air to which the vegetation was exposed. More efficient exchange between plant and

283   atmosphere then results in low storage of CO_2 in the air space below the uppermost height of

284   [CO_2] measurement. At night, subcanopy ventilation by intermittent gusting results in a large

285   variation between negative and positive CO_2 storage.

286   Observations such as these are facilitated by the profile sampling system now

287   advocated. In the future, it is planned to use the new capability to revisit the quality assurance

288   methodology of EC determinations by comparing atmospheric storage to the statistical

289   uncertainty of the covariances. In this context, note that Fig. 5b indicates sensible heat

290 atmospheric storage terms equivalent, on average, to about 2 W m^{-2} in the late morning,

291 followed by a downward trend through the afternoon until reaching a minimum a few hours

292 after sunset. The irregularity seen soon after noon is presently unexplained. Clearly, individual

293 shorter-term averages could display greater averages and increased scatter, but this remains to

294 be explored. In comparison, Finkelstein and Sims (2001) derive uncertainties associated with

295 30-min EC evaluations of the sensible heat covariance in the range 5% to 10% in daytime.
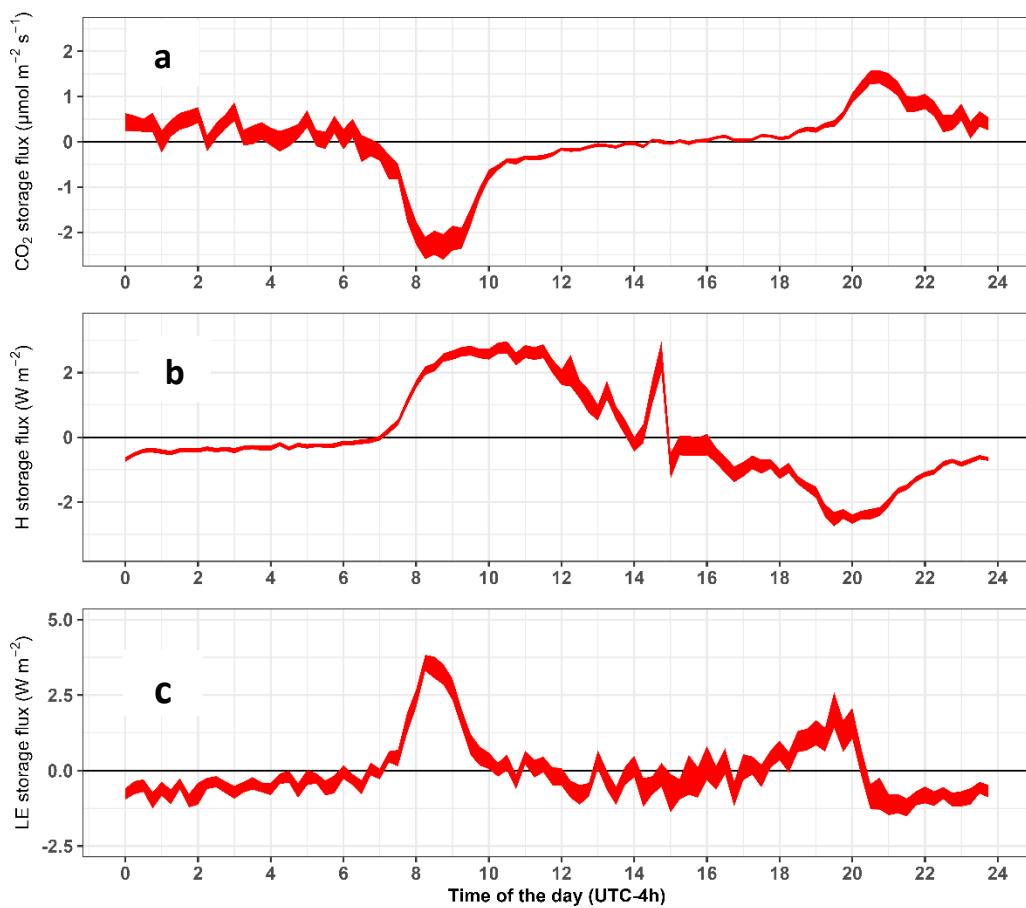
296

297 Fig. 5. Diurnal patterns of CO_2 atmospheric storage (a), sensible heat storage (b) and

298 latent heat storage (c) of the maize crop in early stages of growth (see Table 1 a-b). The

299 widths of the traces correspond to +/- one standard error on the means.

300 The nocturnal sensible (Fig. 5b) and latent (5c) heat energy storages remained low and

301 slightly negative until sunrise, about 0600 LT. As the air cooled during the night, sensible heat

302 storage in the air mass remained slightly negative as its temperature decreased. After sunrise,

303 the air mass warmed and the sensible heat storage rose to a maximum value of about 2 W m^{-2}

304 between 1200 LT and 1230 LT. Afterwards, the sensible heat storage rate declined, reaching

305 negative values a few hours before sunset and attaining a minimum value (about -1.5 W m^{-2}) a

306 few hours before midnight. The sensible heat storage subsequently trended to near-zero

307 constancy until being disrupted by sunrise at about 0700 LT.

308   Latent heat storage (Fig. 5c) fluctuated near zero for most of the daylight hours, after

309 exhibiting a major positive excursion (> 4 W m^{-2}) during the few hours after sunrise. After about

310 2100 LT, latent heat storage fluctuations like the variations seen in Fig. 5a occurred until

311 sunrise, with an average of about -0.5 W m^{-2}. Comparison with Fig. 5a indicates that the post-

312 sunrise increases in latent heat storage coincided with the decrease in CO_2 storage. The

313 sensible heat storage appears to have been delayed by a fraction of an hour. Interpretation of

314 these observations requires consideration of dewfall and its evaporation.

315   Table 1 a-b lists some of the plant growth characteristics during the six–weeks

316 considered here. Also listed are the magnitudes of maximum and minimum storage terms

317 during each of the sampling periods, shown here to exemplify the ability of the new sampling

318 system to reveal such extremes. Detailed examination of the plant-atmosphere interaction for

319 the entire growing season will be presented elsewhere. During the six–week evaluation period,

320 CO_2 atmospheric storage increased as the plant grew and as the soil warmed (increasing

321 heterotrophic CO_2 generation, subsurface) but not substantially; the highest storage rate was

322 found at the VT (tasseling) stage and the minimum at the V2 growth stage, five weeks earlier.

323 Similarly, latent heat storage increased significantly, presumably due to increasing leaf area and

324 transpiration. Latent and sensible heat storage was found higher in the VT growth stage than in

325 other growth stages. As the crop grew, different processes became prominent causes of the

326 storage of energy and CO_2. When the maize was in its early growth stage, the canopy was not

327 fully developed, the soil was cooler, and CO_2 storage did not show much change. However,

328 there were substantial variations in the sensible and latent energy storage terms as the crop

329 grew (see Table 1 a-b).

330 **Table 1 a-b.** Height adjustment during the crop growth stage and maximum and minimum
331 storage terms. V1 is the first leaf emergence, Vn is when the nth leaf fully emerged, and VT is the
332 tasseling stage. Height 1 (H_1) was kept constant throughout the experiment while the other three
333 heights (H_2, H_3, and H_4) changed as the plants grew. Negative and positive signs represent the
334 2.5th percentile (minimum) and 97.5th percentile (maximum) quartile values observed during the
335 different periods.

Table 1 a	Measurement height (m)				Growth stage	Latent heat Storage	Sensible heat storage
Date	H_1	H_2	H_3	H_4		W m^{-2}	W m^{-2}
May 15-May 21	0.11	0.43	0.60	2.00	V2–V3	-15.19 to 6.13	-5.67 to +2.59
May 22-May 28	0.11	0.43	0.60	2.00	V3-V4	-19.45 to +8.16	-5.67 to +3.21
May 29-June 4	0.11	0.43	1.72	3.07	V5-V6	-19.72 to +8.95	-11.65 to +3.74
June 5-June 11	0.11	0.75	2.10	3.12	V6-V7	-19.72 to +9.01	-45.65 to +4.07
June 12-June 18	0.11	0.95	2.50	3.36	V7-V8	-22.72 to +9.36	-45. 65 to +3.68
June 19-June 25	0.11	1.27	3.00	4.36	VT	-22.73 to +9.38	-15.33 to + 4.84

336

337

Table 1 b	Measurement height (m)				Growth stage	CO_2 Storage	Average precipitation	Temperature
Date	H_1	H_2	H_3	H_4		µmol m^{-2} s^{-1}	mm	°C
May 15-May 21	0.11	0.43	0.60	2.00	V2–V3	-7.12 to +2.78	0.00	14.90-25.74
May 22-May 28	0.11	0.43	0.60	2.00	V3-V4	-7.12 to +2.87	0.031	14.59-26.63
May 29-June 4	0.11	0.43	1.72	3.07	V5-V6	-9.54 to +2.59	0.007	14.17-28.12
June 5-June 11	0.11	0.75	2.10	3.12	V6-V7	-9.67 to + 2.33	0.165	12.87-29.70
June 12-June 18	0.11	0.95	2.50	3.36	V7-V8	-9.68 to +2.36	0.081	13.41-29.12
June 19-June 25	0.11	1.27	3.00	4.36	VT	-6.23 to +2.57	0.00	19.22-26.46

338

339

340

4. Conclusions

The field evaluation of the multi-port profile system demonstrated its effectiveness in measurement of CO_2 and H_2O concentrations at different heights within the surface roughness layer. The multiple-height profile system aided substantially to understanding CO_2 and H_2O concentration variations and their vertical profiles, thereby facilitating precise assessments of their exchanges, storage, and overall balance within the growing maize ecosystem. The observations reveal that different processes became prominent at different growth stages, which influenced the atmospheric storage of heat energy and gas and the associated fluxes as the canopy developed. An issue remaining to be addressed is that condensation of water in the sampling tubes was sometimes observed; this will affect measurement accuracy and steps to eliminate the problem are presently being reviewed.

The 2023 field experience with the new system indicates that canopy data obtained from the vertical profile observations offer potential for many applications in future studies such as evaluation of soil-plant-atmospheric models that rely on the precise estimation of CO_2, heat and water vapor fluxes. Note that the definition of the heat storage used here (as in Eq. (2)) omits warming of the biomass. This omission accounts for the differences between the storage terms now computed and those published previously (e.g., Hicks et al., 2022).

The simplicity of the sampling system device contributes to its success — it suffered a few disruptions during the testing period. This new measurement system will be employed in future studies of air-surface exchange when moderated by the presence of a crop and especially when operation in remote locations is required. Measurements made will permit improved quantification of storage terms — atmospheric, biological, in the soil, and all contributing to a better understanding of the surface heat energy balance. Sub-canopy measurements, in particular, will help track how respiration, evaporation, photosynthesis, etc. vary through the depth of the canopy. Such studies will also help to evaluate micrometeorological models, such as those describing the variation of gases, temperature, and water vapor within a canopy. This new device is now being used for the assessment of canopy gas emissions, starting with carbon dioxide but in the future intended to include nitrous oxide.

369 In summary, this new device has the potential to improve our understanding of soil-plant-

370 atmosphere interactions, particularly within the plant canopies.

371 **Author contribution statement**

372 **TR:** Data curation, Formal analysis, Methodology, Visualization, Writing – original draft. **BBH:** Supervision,

373 Methodology, Visualization, Writing – revision and editing. **NSE:** Supervising, Funding acquisition, Project

374 administration, Writing – review & editing. **JNO:** Formal analysis, writing and reviewing.

375 **Funding**

376 This work was supported by DuPont Tate & Lyle Bio Products Company.

377 **Declaration of competing intertest**

378 Authors declare no competing interest associated with this submission.

379 **Acknowledgment**

380 This work was supported by the University of Tennessee, Knoxville. The authors thank David R.

381 Smith (Senior Technical Specialist, BESS, UTK), Wesley C. Wright (Senior Research Associate,

382 BESS, UTK), Scott Karas Trucker (Senior Technical Specialist, BESS, UTK) and Josh Watson

383 (Farmer) for their support.

384 **References**

385 Davidson, E., and Janssens, I.: Temperature sensitivity of soil carbon decomposition and feedbacks

386   to climate change. Nature, 440, 165–173, https://doi.org/10.1038/nature04514, 2006.

387 Eash, N.S., O'Dell, D., Sauer, T.J., Hicks, B.B., Lambert, D.L. and Thierfelder, C.: Real-time carbon

388   sequestration rates on smallholder fields in Southern Africa. Institute of Agriculture,

389   University of Tennessee, Knoxville, TN., 2013.

390 Finkelstein, P.L. and Sims, P.F.: Sampling error in eddy correlation flux measurements. J.

391   Geophys. Res.: Atmospheres, 106(D4), 3503–3509,

392   https://doi.org/10.1029/2000JD900731, 2001.

393 Finnigan, J.: The storage flux in eddy flux calculations, Agric. For. Meteorol., 136(3–4), 108–113,

394   https://doi.org/10.1016/j.agrformet.2004.12.010, 2006.

395 Galmiche, M. and J. C. R. Hunt.: The formation of shear and density layers in stably stratified

396   turbulent flows: linear processes. J. Fluid Mech., 455, 243–262,

397   https://doi.org/10.1017/S002211200100739X, 2002.

398 Hicks, B.B., Eash, N.S., O'Dell, D.L. and Oetting, J.N.: Augmented Bowen ratio analysis I: site

399   adequacy, fetch and heat storage (ABRA), Agric. For. Meteorol., 290, 108035,

400   https://doi.org/10.1016/j.agrformet.2020.108035, 2020.

401 Hicks, B.B., Lichiheb, N., O'Dell, D.L., Oetting, J.N., Eash, N.S., Heuer, M. and Myles, L.: A

402   statistical approach to surface renewal: The virtual chamber concept. Agrosys. Geosci.

403   Environ., 4(1), p.ee20141, https://doi.org/10.1002/agg2.20141, 2021.

404 Hicks, B.B., Oetting, J.N., Eash, N.S. and O'Dell, D.L.: Augmented Bowen ratio analysis, II: Ohio

405   comparisons. Agric. For. Meteorol., 313, 108760,

406   https://doi.org/10.1016/j.agrformet.2021.108760, 2022.

407 Hoeltgebaum, L.E.B. and Nelson L.D.: Evaluation of the storage and evapotranspiration terms of

408   the water budget for an agricultural watershed using local and remote-sensing

409   measurements, Agric. For. Meteorol., 341, 109615,

410   https://doi.org/10.1016/j.agrformet.2023.109615, 2023.

411 Lamas Galdo, M.I., Rodriguez García, J.D. and Rebollido Lorenzo, J.M.: Numerical model to

412   analyze the physicochemical mechanisms involved in CO_2 absorption by an aqueous

413   ammonia droplet. Int. J. Environ. Res. Public Health, 18(8), p.4119,

414   https://doi.org/10.3390/ijerph18084119, 2021.

415 Leuning, R.: Estimation of scalar source/sink distributions in plant canopies using lagrangian

416   dispersion analysis: corrections for atmospheric stability and comparison with a

417   multilayer canopy model, Boundary Layer Meteorol., 96:293–314,

418   https://doi.org/10.1023/A:1002449700617, 2012.

419   Massman, W. and Lee, X.: Eddy covariance flux corrections and uncertainties in long-flux

420   studies of carbon and energy exchanges, Agric. For. Meteorol., 113(1–4), 121–144,

421   https://doi.org/10.1016/S0168-1923(02)00105-3, 2002.

422   Mayocchi, C.L. and Bristow, K.L.: Soil surface heat flux: some general questions and comments

423   on measurements, Agric. For. Meteorol., 75(1–3), 43–50 (1995).

424   https://doi.org/10.1016/0168-1923(94)02198-S, 1995.

425   McCaughey, J.H. and Saxton, W.L.: Energy balance storage fluxes in a mixed forest, Agric. For.

426   Meteorol., 44(1), 1–18, https://doi.org/10.1016/0168-1923(88)90029-9, 1988.

427   Meyers, T. P. and Hollinger, S. E.: An assessment of storage terms in the surface energy balance

428   of maize and soybean, Agric. For. Meteorol., 125(1–2), 105–115,

429   https://doi.org/10.1016/j.agrformet.2004.03.001, 2004.

430   Montagnani, L., Grünwald, T., Kowalski, A., Mammarella, I., Merbold, L., Metzger, S., Sedlák, P.

431   and Siebicke, L.: Estimating the storage term in eddy covariance measurements: the

432   ICOS methodology, Int. Agrophysics., 32 (4), 551–567, https://doi: 10.1515/intag-2017-

433   0037, 2018.

434   Nicolini, G., Aubinet, M., Feigenwinter, C., Heinesch, B., Lindroth, A., Mamadou, O., Moderow,

435   U., Mölder, M., Montagnani, L., Rebmann, C. and Papale, D.: Impact of CO_2 storage flux

436   sampling uncertainty on net ecosystem exchange measured by eddy covariance. Agri.

437   For. Meteorol., 248, 228–239, http://dx.doi.org/10.1016/j.agrformet.2017.09.025, 2018.

438   O'Dell, D., Sauer, T.J., Hicks, B.B., Thierfelder, C., Lambert, D.M., Logan, J. and Eash, N.S.: A

439   short-term assessment of carbon dioxide fluxes under contrasting agricultural and soil

440   management practices in Zimbabwe. J. Agri. Sci. 7(3),

441   http://dx.doi.org/10.5539/jas.v7n3p32, 2015.

442   O'Dell, D., Sauer, T.J., Hicks, B.B., Lambert, D.M., Smith, D.R., Bruns, W.A., Basson, A., Marake,

443   M.V., Walker, F., Wilcox, M.D. and Eash, N.S.: Bowen ratio energy balance measurement

444   of carbon dioxide (CO_2) fluxes of no-till and conventional tillage agriculture in Lesotho.

445   Open J. Soil Sci. 4(3): 87–97, http://hdl.handle.net/10919/70228, 2014.

446 Oetting, J., Hicks, B. and Eash, N.: On recursive partitioning to refine coordinate rotation in Eddy
447   covariance applications. Agri. For. Meteorol., 1;346:109873,
448   https://doi.org/10.1016/j.agrformet.2023.109873, 2024.

449 Papale, D., Reichstein, M., Aubinet, M., Canfora, E., Bernhofer, C., Kutsch, W. and Yakir, D.:
450   Towards a standardized processing of Net Ecosystem Exchange measured with eddy
451   covariance technique: algorithms and uncertainty estimation, Biogeosci., 3(4), 571–583,
452   https://doi.org/10.5194/bg-3-571-2006, 2006.

453 Pastorello, G., Trotta, C., Canfora, E., Chu, H., Christianson, D., Cheah, Y.W., Poindexter, C.,
454   Chen, J., Elbashandy, A., Humphrey, M. and Isaac, P.: The FLUXNET2015 dataset and the
455   ONEFlux processing pipeline for eddy covariance data. Sci. Data, *7*(1), 225,
456   https://doi.org/10.6084/m9.figshare.12295910, 2020.

457 Raza, T., Oetting, J., Eash, N., Hicks, B. and Lichiheb, N.: Assessing energy balance closure over
458   maize canopy using multiport system and canopy net storage, in: Proceedings of the
459   104th AMS Annual Meeting, Baltimore, Maryland, USA, 28 January to 1 February, 2024.

460 Raza, T., Hicks, B., Oetting, J. and Eash, N.: On the agricultural eddy covariance storage term:
461   measuring carbon dioxide concentrations and energy exchange inside a maize canopy,
462   in: Proceedings of the 103rd AMS Annual Meeting, Denver, Colorado, USA, 8–12
463   January, 2023.

464 Russell, E.S., Liu, H., Gao, Z., Finn, D. and Lamb, B., Impacts of soil heat flux calculation methods
465   on the surface energy balance closure. Agricultural and Forest Meteorology, 214, 189–
466   200, https://doi.org/10.1038/nature04514, 2015.

467 Ryan, M., Law, B. Interpreting, measuring, and modeling soil respiration. Biogeochemistry 73,
468   3–27, https://doi.org/10.1007/s10533-004-5167-7, 2005.

469 Twine, T.E., Kustas, W.P., Norman, J.M., Cook, D.R., Houser, P.R., Meyers, T.P., Prueger, J.H.,
470   Starks, P.J. and Wesely, M.L.: Correcting eddy-covariance flux underestimates over a

471   grassland, Agric. For. Meteorol., 103 (3), 279–300, https://doi.org/10.1016/S0168-

472   1923(00)00123-4, 2000.

473   USDA-NRCS (2018). Soil Survey Staff, Natural Resources Conservation Service, United States

474   Department of Agriculture. Web Soil Survey. Available at:

475   https://websoilsurvey.sc.egov.usda.gov/App/WebSoilSurvey.aspx, Accessed November

476   2018.

477   Varmaghani, A., Eichinger, W.E. and Prueger, J.H.: A diagnostic approach towards the causes of

478   energy balance closure problem. Open J. Mod. Hydrol., 6(02), 101,

479   https://doi.org/10.4236/ojmh.2016.62009, 2016.

480   Verma, S.B. and Rosenberg, N.J.: Vertical profiles of carbon dioxide concentration in stable

481   stratification. Agric. Meteorol, 16(3), 359–369, https://doi.org/10.1016/0002-

482   1571(76)90005-4, 1976.

483   Wang, X., Zhong, L., Ma, Y., Fu, Y., Han, C., Li, P., Wang, Z. and Qi, Y.: Estimation of hourly actual

484   evapotranspiration over the Tibetan Plateau from multi-source data. Atmos. Res., 281,

485   106475, https://doi.org/10.1016/j.atmosres.2022.106475, 2023.

486   Wilson, K.B., Goldstein, A., Falge, E., Aubinet, M., Baldocchi, D., Berbigier, P., Bernhofer, C.,

487   Ceulemans, R., Dolman, H., Field, C., Grelle, A., Ibrom, A., Law, B., Kowalski, A., Meyers,

488   T., Moncrieff, J., Monson, R., Oechal, W., Tenhunen, J., Valentini, R. and Verma, S.:

489   Energy balance closure at FLUXNET sites, Agric. For. Meteorol., 113, 223–243,

490   https://doi.org/10.1016/S0168-1923(02)00109-0, 2002.